



# CT radiomics nomogram for the preoperative prediction of lymph node metastasis in gastric cancer

Yue Wang<sup>1</sup> · Wei Liu<sup>1</sup> · Yang Yu<sup>2</sup> · Jing-juan Liu<sup>1</sup> · Hua-dan Xue<sup>1</sup> · Ya-fei Qi<sup>1</sup> · Jing Lei<sup>1</sup> · Jian-chun Yu<sup>3</sup> · Zheng-yu Jin<sup>1</sup>

Received: 25 March 2019 / Revised: 8 July 2019 / Accepted: 26 July 2019 / Published online: 29 August 2019  
© European Society of Radiology 2019

## Abstract

**Purpose** To investigate the role of computed tomography (CT) radiomics for the preoperative prediction of lymph node (LN) metastasis in gastric cancer.

**Materials and methods** This retrospective study included 247 consecutive patients (training cohort, 197 patients; test cohort, 50 patients) with surgically proven gastric cancer. Dedicated radiomics prototype software was used to segment lesions on preoperative arterial phase (AP) CT images and extract features. A radiomics model was constructed to predict the LN metastasis by using a random forest (RF) algorithm. Finally, a nomogram was built incorporating the radiomics scores and selected clinical predictors. Receiver operating characteristic (ROC) curves were used to validate the capability of the radiomics model and nomogram on both the training and test cohorts.

**Results** The radiomics model showed a favorable discriminatory ability in the training cohort with an area under the curve (AUC) of 0.844 (95% CI, 0.759 to 0.909), which was confirmed in the test cohort with an AUC of 0.837 (95% CI, 0.705 to 0.926). The nomogram consisted of radiomics scores and the CT-reported LN status showed excellent discrimination in the training and test cohorts with AUCs of 0.886 (95% CI, 0.808 to 0.941) and 0.881 (95% CI, 0.759 to 0.956), respectively.

**Conclusions** The CT-based radiomics nomogram holds promise for use as a noninvasive tool in the individual prediction of LN metastasis in gastric cancer.

## Key Points

- CT radiomics showed a favorable performance for the prediction of LN metastasis in gastric cancer.
- Radiomics model outperformed the routine CT in predicting LN metastasis in gastric cancer.
- The radiomics nomogram holds potential in the individualized prediction of LN metastasis in gastric cancer.

**Keywords** Gastric cancer · Radiomics · Nomogram

✉ Jian-chun Yu  
yu-jch@163.com

✉ Zheng-yu Jin  
jinzy@pumch.cn

<sup>1</sup> Department of Radiology, Peking Union Medical College Hospital, Chinese Academy of Medical Sciences and Peking Union Medical College, No. 1, Shuaifuyuan, Dongcheng District, Beijing 100730, People's Republic of China

<sup>2</sup> CT Collaboration, Siemens Healthineers Ltd., 59# Beizhan Road, Shenyang 110013, People's Republic of China

<sup>3</sup> Department of General Surgery, Peking Union Medical College Hospital, Chinese Academy of Medical Sciences and Peking Union Medical College, No. 1, Shuaifuyuan, Dongcheng District, Beijing 100730, People's Republic of China

## Abbreviations

AP	Arterial phase
AUC	Area under the curve
CART	Classification and regression tree
CT	Computed tomography
DCA	Decision curve analysis
DICOM	Digital Imaging and Communications in Medicine
ICC	Intraclass correlation coefficient
GLCM	Gray-level co-occurrence matrix
GLRLM	Gray-level run-length matrix
LN	Lymph node
MRI	Magnetic resonance imaging
NAC	Neoadjuvant chemotherapy

RF	Random forest
ROC	Receiver operating characteristics
VOI	Volume of interest

## Introduction

Although its incidence has been significantly reduced over the past decades, gastric cancer is still the third leading cause of cancer-related death worldwide [1]. Lymph node (LN) metastasis is one of the main prognostic factors for gastric cancer, and it plays a pivotal role in the selection of appropriate candidates for neoadjuvant chemotherapy (NAC) therapy [2–5]. NAC is recommended for locally advanced cases only in the presence of bulky LN metastasis according to the newly published Japanese Gastric Cancer Guidelines (Ver5) [5, 6]. A prospective multi-institutional validity study carried out by the Japan Clinical Oncology Group proposed to add LN metastasis as a criterion for the selection of patients to receive NAC therapy [2]. Thus, an accurate prediction of LN metastasis in gastric cancer is crucial for clinical decision-making and the improvement of prognosis. Traditional methods for determining nodal status using imaging tools are mainly based on the size of the LNs. However, reactive or inflammatory LNs can be enlarged, normal-sized, or minimally enlarged nodes accounting for a considerable proportion of malignance. Hence, a proportion of patients are at high risk for inaccurate clinical nodal staging [7–9]. Computed tomography (CT) is the most commonly used imaging modality for the preoperative assessment of LN status, but the reported accuracy was unsatisfactory, only at approximately 60% [7, 10].

An alternative, noninvasive technique is needed to supplement the routinely used imaging tools. As a previous study revealed, tumors with a poor differentiation degree, vascular invasion, and epidermal growth factor receptor overexpression were reported to be more prone to LN metastasis [11–13]. In this case, another strategy to evaluate the LN status can be relied on the comprehensive characteristics of the primary lesion. However, most of those features can only be obtained from postoperative pathological examination. Radiomics is an emerging field that allows a noninvasive approach to extract quantitative features from medical images [14–16], which has exhibited great potential in oncological practice, including differentiation diagnosis, prediction of histological classification, LN metastasis, therapeutic response, and prognosis [17–26]. Currently, studies of radiomics in the prediction of LN metastasis in gastric cancer are rare, and most of which are MRI-based approaches [20, 21]. The purpose of this study was to investigate the role of radiomics derived from

standard-of-care CT images in the prediction of LN metastasis in gastric cancer.

## Materials and methods

### Patients

This retrospective study was approved by the institutional review board with a waiver of written informed consent. A total of 247 patients (167 males and 80 females; mean age,  $60.7 \pm 11.2$  years) with pathologically proven gastric cancer were consecutively enrolled at our institution between June 2014 and November 2018. The inclusion criteria entailed pathologically confirmed gastric cancer with definite LN stage, without NAC before surgery, and preoperative enhanced abdominal CT examination within 2 weeks prior to the operation. The exclusion criteria were as follows: received NAC or radiotherapy before surgery, image quality was insufficient for diagnosis due to artifacts or poor distention, lack of definite information on postoperative LN status, and small lesions that were hardly visible on CT images. Demographical data, clinical information, and pathological node stage were derived from medical records. Although distant LN metastasis should be classified as M1 [27], these patients were also included and labeled as positive LN metastasis as the study mainly focused on the prediction of the presence of LN metastasis. We hypothesized that the radiomics model can improve the accuracy for the prediction of LN metastasis to be 82.3% [20], given that the reported accuracy was 64% for routine CT [10]; the sample size estimation formula revealed that 73 patients would ensure us to have 95% confidence and 80% power to detect the expected superiority of radiomics [28]. Considering the primary purpose of the study was to construct a radiomics model for prediction of LN metastasis based on the retrospectively collected CT images, all eligible subjects were kept as inclusion of large population which was recommended in radiomics study to provide more power for the predictive classifier [29].

### CT examination and CT-reported LN status

The CT examination was performed using two 64-channel CT (Discovery CT750, GE Medical Systems; IQon-Spectral, Philips) and one dual-source CT (SOMATOM Definition Flash, Siemens) vendors. Patients were required to fast for no less than 6 h. Before the CT scan, all patients drank approximately 1000 ml of water to distend the stomach. In addition, 20 mg of anisodamine was injected intravenously to avoid gastric peristalsis. Patients were required to hold their breath while the examination was performed. Following the unenhanced scan, patients were infused with 1.5 ml/kg of nonionic contrast material (Ultravist 370, Bayer Schering

Pharma) at a rate of 3.0 ml/s into the antecubital vein using an automatic pump injector. Arterial phase (AP), portal phase, and delay phase contrast-enhanced images were acquired at 25–30-s, 65–70-s, and 110–120-s delay after the injection of contrast material, respectively. The other acquisition parameters included the following: tube voltage of 80 to 120 kVp; tube current of 120 to 640 mA; detector collimation of 0.625 or 0.6 mm; image matrix of  $512 \times 512$ ; and reconstruction slice thickness of 0.625 mm or 1 mm. Two experienced abdominal radiologists reviewed the CT images to evaluate the presence of LN metastasis in consensus blinded to the pathological information. Any disagreement was resolved by consultation. LN metastasis was established if the short-axis diameter was larger than 6 mm for perigastric LN and larger than 8 mm for extraperigastric LN [7].

### Tumor segmentation and feature extraction

Tumor segmentation was performed by using a dedicated semi-processing prototype software “Radiomics” (syngo.via Frontier, Version 1.0.0, Siemens). One radiologist with a 6-year experience in abdominal radiology segmented the lesions of all subjects. A senior radiologist (15-year experience in abdominal radiology) segmented 50 cases with 25 pathologically proven LN metastasis and 25 free of LN metastasis randomly selected from all samples to evaluate the inter-operator variability. When performing the segmentation, the radiologists were informed of the proven surgical locations of the tumor but were blinded to other clinical information and pathologic results. It seems that the performance of texture features extracted from AP images was slightly better than those from portal phase images in prior studies [17, 19]. Therefore, the current study retrieved AP enhanced images of Digital Imaging and Communications in Medicine (DICOM) format for radiomics feature extraction. The entire volume of the lesion was segmented semi-automatically. The contours were drawn carefully to avoid involving adjacent fluid or air. The top and bottom slices were also excluded to reduce bias caused by partial volume effects. A total of 844 radiomics features were extracted from the volume of interest (VOI). Four types of radiomics features were obtained: (1) 16 shape and size features, features related to the three-dimensional size and shape of the tumor; (2) 18 first-order statistics, features about the distribution of voxel intensities within the selected region; (3) 74 texture-based features, features describing patterns or the spatial distribution of voxel intensities, which were calculated from gray-level co-occurrence matrix (GLCM) and gray-level run-length matrix (GLRLM). Voxel intensities were resampled into equally spaced bins using a bin-width of 25 HU, as the discretization of the voxel intensity values within the VOI was necessary to determine texture matrix representations. Discretization not only reduces image noise but also normalizes intensities across all patients, allowing a

direct comparison of all calculated textural features between patients; (4) 736 wavelet features, wavelet decompositions of first-order statistics and texture features. Wavelet transform effectively decouples textural information by decomposing the original image in a manner similar to the Fourier analysis in low and high frequencies. Figure 1 showed the workflow of tumor segmentation and feature extraction.

### Building up the radiomics model

Radiomics model was built with our in-house software programmed with the Python Scikit-learn package (Python version 3.7, Scikit-learn version 0.21, <http://scikit-learn.org/>). All patients were first split into training cohort and test cohort with a ratio of 8:2 by using the random series generated by the computer [30, 31]: 197 patients (mean age,  $61.0 \pm 10.9$  years; positive LN metastasis, 146 cases; negative LN metastasis, 51 cases) were allocated into the training cohort; 50 patients (mean age,  $59.5 \pm 12.6$  years; positive LN metastasis, 37 cases; negative LN metastasis, 13 cases) were allocated into the test cohort. A popular data-preprocessing method in machine learning—random under-sampling algorithm—was applied to the training cohort to handle the imbalance between LN statuses (positive vs negative, 146/51) with the purpose of avoiding bias toward majority class cases and achieving a high classification rate [32]. Random forest (RF) method was used to construct the prediction model because of its high variance-bias trade-off capability. Features with intraclass correlation coefficient (ICC) value higher than 0.8 were considered stable and selected for model construction [33, 34]. Further feature selection was skipped for the sake of its help in reducing computational time more than improving the prediction accuracy when using RF method [35]. RF ensembles are a series of decision trees that act as weak classifiers individually yet form a robust prediction in aggregate. This method would randomly draw bootstrap samples and features for the establishment of each classification and regression tree (CART). Each time, 2/3 of all data sets and the square root of total features were randomly selected with replacement for the training process. Gini impurity was used for splitting the branches. The final prediction was made by voting or averaging using the bagging method. A fivefold cross-validation was utilized to improve the model performance [30]. Hyperparameters in the study including the number of trees in the forest and the minimum sample limitation for leaf node were optimized through the cross-validation process. Finally, the best model was selected and validated on the test cohort. Predicted LN status and radiomics score for each case were recorded.

### Radiomics nomogram construction

All available clinical variables, including age, gender, location of the tumor, tumor morphology, laboratory tests,

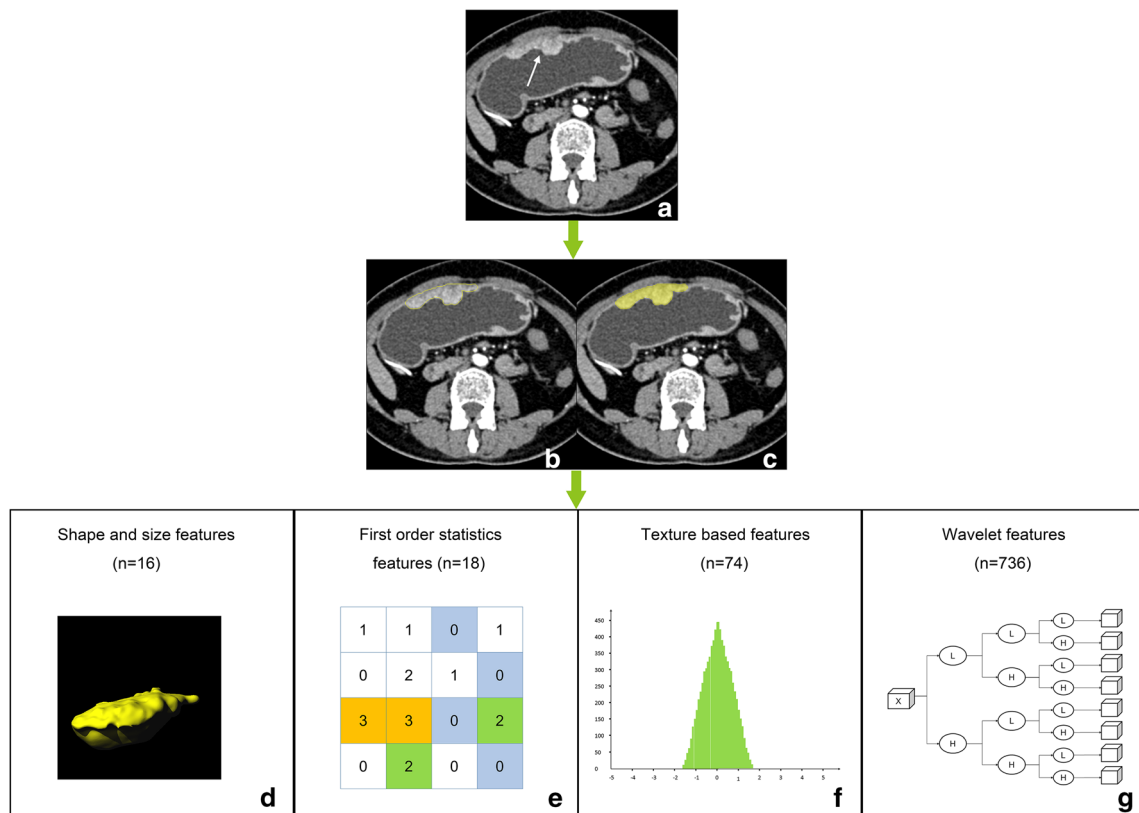


**Fig. 1** Work flow of tumor segmentation and feature extraction. **a** Axial AP enhanced CT images shows the tumor (white arrow). **b, c** Tumor segmentation. The edge of the lesion is drawn carefully to avoid

involving adjacent fluid or air (**b**). The yellow area represents the selected region on the slice (**c**). **d–g** Extraction of four categories of radiomics features

CT-reported LN status, and radiomics scores, were evaluated with a univariate logistic regression algorithm in the training set. Variables with  $p < 0.2$  from univariate analysis were included for further application in a multivariate logistic regression algorithm using forward stepwise selection. Likelihood ratio test based on the maximum partial likelihood estimates was applied to select the significant predictors for LN metastasis. Finally, a radiomics nomogram was constructed based on the multivariate logistic regression model incorporating the selected predictors with the R software package (version 3.5.2: <http://www.Rproject.org>).

**Statistical analysis**

Statistical analysis was performed with SPSS software (version 19), SAS (version 9.2), R software package (version 3.5.2: <http://www.Rproject.org>), and the Python Scikit-learn package (version 3.7, Scikit-learn Version 0.21, <http://scikit-learn.org/>). Qualitative variables were presented as frequencies. Differences between qualitative variables were compared with the chi-square test. The continuous variables were tested for normality by using

the Kolmogorov-Smirnov test. Normally distributed variables were shown as the mean  $\pm$  SD (standard deviation). Differences between normally distributed variables were compared with  $t$  test. Data were presented as the median and interquartile range (IQR) when the variables were nonnormally distributed, and differences between these variables were analyzed with the Mann-Whitney  $U$  test. Inter-operator variability of the radiomics features was assessed with ICC. Violin plot—a hybrid of a box plot and kernel density plot—was used to illustrate the distribution of the radiomics scores and its probability density in both cohorts [36]. The performance of the radiomics model and nomogram in both cohorts were evaluated with receiver operator characteristics (ROC) curves. The ROCs of the radiomics model in the two cohorts were compared with the DeLong test to evaluate whether overfitting occurred. The calibration of the radiomics nomogram was assessed with a calibration curve. The goodness-of-fit of the nomogram in both cohorts was assessed with the Osious test, McCullagh test, and Hosmer-Lemeshow test, respectively. Decision curve analysis (DCA) was performed to determine the clinical usefulness of the radiomics model and nomogram by calculating the net

**Table 1** Clinical characteristics in the training and test cohorts

Clinical characteristics	Training cohort (n = 197)		Test cohort (n = 50)		p§
	LN (-), (n = 51)	LN(+), (n = 146)	LN (-), (n = 13)	LN (+), (n = 37)	
		$p_a$		$p_b$	
Age (years), (mean ± SD)	62.2 ± 9.6	60.5 ± 11.3	61.2 ± 9.5	58.9 ± 13.5	0.393
Gender, n (%)					
Female	14 (27.45)	52 (35.62)	3 (23.08)	11 (29.73)	0.573
Male	37 (72.55)	94 (64.38)	10 (76.92)	26 (70.27)	0.920
Tumor location, n (%)					
Fundus	9 (17.65)	17 (11.65)	3 (23.08)	4 (10.81)	0.130
Body	7 (13.73)	45 (30.82)	2 (15.38)	11 (29.73)	
Antrum	35 (68.62)	84 (57.53)	8 (61.54)	22 (59.46)	
Flat	44 (86.27)	117 (80.14)	11 (84.62)	25 (67.57)	0.882
Ulceration	7 (13.73)	29 (19.86)	2 (15.38)	12 (32.43)	0.893
Laboratory tests, median (IQR)					
Neutrophil ( $10^9/L$ )	4.47 (3.10, 9.12)	4.21 (2.79, 6.22)	4.47 (3.05, 6.62)	4.01 (3.03, 5.19)	0.701
Lymphocyte ( $10^9/L$ )	1.48 (1.09, 1.85)	1.40 (1.02, 1.84)	1.56 (1.16, 1.89)	1.53 (0.95, 1.78)	0.666
NLR	3.98 (1.68, 6.59)	2.46 (1.75, 6.50)	2.33 (1.73, 3.20)	2.74 (1.98, 4.59)	0.892
Albumin (g/L)	38 (35, 42)	40 (36, 43)	43 (39, 45)	39 (34, 42)	0.711
Pathological N stage, n (%)					
0	51 (100)	-	13 (100)	-	0.008*
1	-	27 (18.49)	-	11 (29.73)	0.987
2	-	38 (26.03)	-	6 (16.22)	
3a	-	55 (37.67)	-	13 (35.14)	
3b	-	26 (17.81)	-	7 (18.92)	
CT-reported LN status, n (%)					
LN (-)	40 (78.43)	63 (43.15)	11 (84.62)	17 (45.95)	0.911‡
LN (+)	11 (21.57)	83 (56.85)	2 (15.38)	20 (54.05)	

Note: LN (-) : lymph node metastasis negative; LN(+): lymphnode metastasis positive; NLR: neutrophil to lymphocyte ratio;  $p_a$ :  $p$  value of comparison between LN (-) and LN (+) in training cohort;  $p_b$ :  $p$  value of comparison between LN (-) and LN (+) in test cohort; §: comparison between the training cohort and test cohort; ‡: comparison of accuracy by CT-reported LN status between training and test cohort; SD: standard deviation; IQR:interquartile ranges; \*:  $p < 0.05$ ;

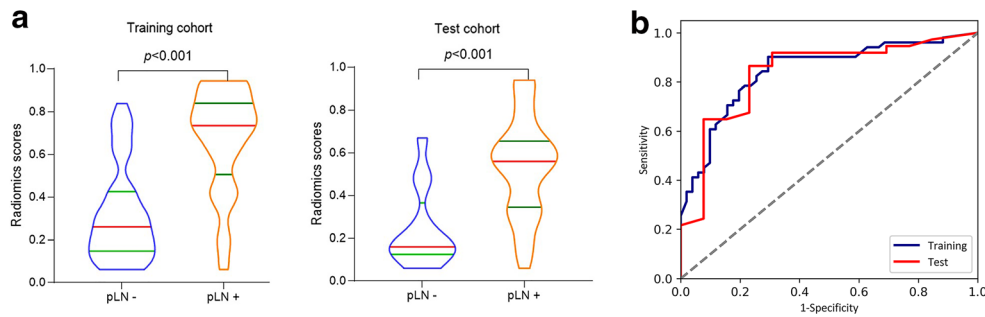


**Fig. 2** a Violin plot of the radiomics scores in the training cohort and test cohort. pLN -, pathological negative LN metastasis; pLN +, pathological positive LN metastasis. The difference between radiomics scores was compared with *t* test. Wider sections of the plot represent a higher

probability that patients of the group would take on the given value; skinnier sections represent a lower probability. The red lines represent the median value. The green lines represent the interquartile. b ROC curves of the radiomics model in the training and test cohort

benefits at different threshold probabilities in the training and test cohort. The net benefit is equivalent to the proportion of net true positives in brief [37].

cohort and 62% in the test cohort ( $p = 0.911$ ). Details of the demographical data and clinical characteristics of the training and test cohorts were summarized in Table 1.

## Results

### Clinical characteristics

Among the 247 eligible patients, 183 patients had LN metastasis (181 patients with regional LN metastasis and 2 patients with distant LN metastasis); the rest 64 patients showed negative LN metastasis. Except for the level of albumin in patients with LN metastasis being lower than those with negative LN metastasis in the test cohort, no significant differences were found between patients with positive and negative LN metastasis in both cohorts in terms of age, gender, tumor location, tumor morphology, or the other laboratory tests. The accuracy of routine CT in the diagnosis of LN metastasis was 62.4% in the training

### Radiomics model building and evaluation

Altogether 150 radiomics features were shown to be stable, including 9 shape and size features, 11 first-order features, 35 texture features, and 95 wavelet features. To take the effects of scanning parameters and patient variance into consideration, the radiomics model was built based on 5 general features (scanning kilo-voltage, tube current, slice thickness, patient age, and gender) as well as these 150 radiomics features. The radiomics scores in patients with LN metastasis were significantly higher than those with negative LN both in the training cohort ( $0.67 \pm 0.24$  vs  $0.32 \pm 0.22$ ,  $p < 0.001$ ) and test cohort ( $0.53 \pm 0.23$  vs  $0.24 \pm 0.19$ ,  $p < 0.001$ ). The violin plot of the radiomics scores in both cohorts was displayed in Fig. 2a. The radiomics model showed a favorable discriminatory ability in the training cohort with an area under the curve (AUC) of 0.844 (95% CI, 0.759 to 0.909), which was confirmed in the test cohort with an AUC of 0.837 (95% CI, 0.705 to 0.926) (Fig. 2b). There was no significant difference in ROCs between the two cohorts (DeLong test,  $p = 0.9002$ ). The accuracy of the radiomics model was 80% (sensitivity, 90%; specificity, 71%) in the training cohort and 84% (sensitivity, 86%; specificity, 77%) in the test cohort. The radiomics model outperformed the conventional routine CT in the prediction of LN metastasis (training cohort, 80% vs 62.4%; test cohort, 84% vs 62%).

**Table 2** Results of univariate and multivariate regression analysis

Characteristics	<i>pu</i>	<i>pm</i>
Age	0.343	–
Gender	0.146*	0.96
Location of tumor	0.418	–
Tumor morphology	0.780	–
Neutrophil (109/L)	0.306	–
Lymphocyte (109/L)	0.185*	0.451
NLR	0.171 *	0.818
Albumin (g/L)	0.358	–
CT-reported LN status	0.000*	0.002 <sup>§</sup>
Radiomics scores	0.000*	0.000 <sup>§</sup>

*pu*, *p* value of univariate analysis; *pm*, *p* value of multivariate analysis; *NLR*, neutrophil to lymphocyte ratio. \* $pu < 0.2$ ; <sup>§</sup>  $pm < 0.05$

### Construction and validation of radiomics nomogram

The results of the univariate and multivariate regression analysis were summarized in Table 2. Multivariable analysis revealed that radiomics scores and CT-reported LN

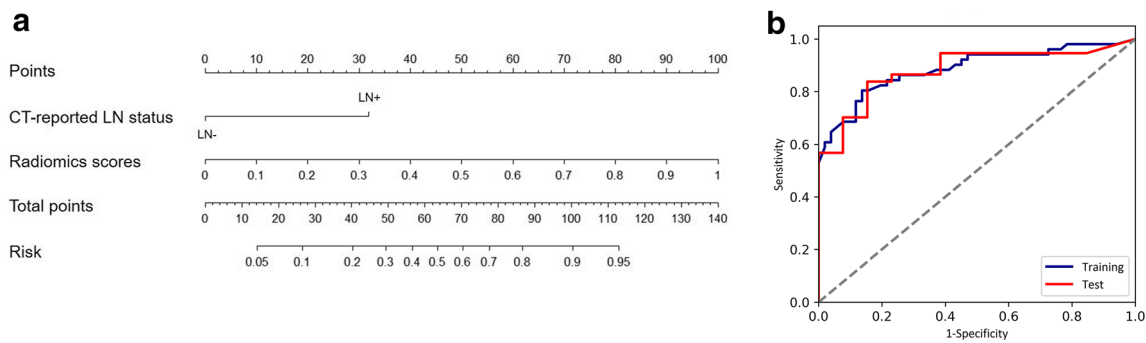


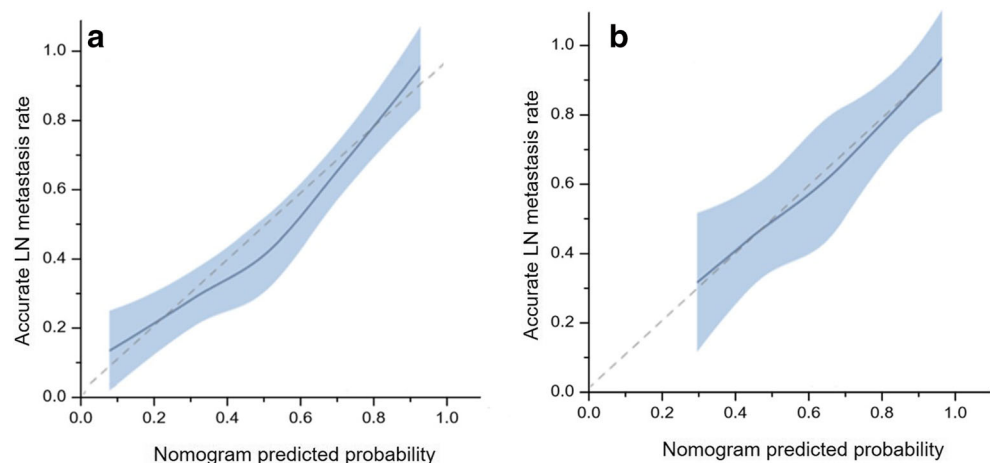
**Fig. 3** **a** CT-based radiomics nomogram for the prediction of LN metastasis in patients with gastric cancer. **b** ROC curves of the radiomics nomogram in the training and test cohorts

status were significant independent factors of LN metastasis. A quantitative nomogram incorporating these two variables was built to predict the individual LN status (Fig. 3a). The nomogram showed good performance for discriminating LN metastasis with AUCs of 0.886 (95% CI, 0.808 to 0.941) and 0.881 (95% CI, 0.759 to 0.956) in the training and test cohorts, respectively (Fig. 3b). The Osius test (training cohort,  $p = 0.688$ ; test cohort,  $p = 0.707$ ), McCullagh test (training cohort,  $p = 0.674$ ; test cohort,  $p = 0.652$ ), and Hosmer-Lemeshow test (training cohort,  $p = 0.210$ ; test cohort,  $p = 0.822$ ) yielded nonsignificant  $p$  values in both cohorts indicating that the nomogram was acceptable. Figure 4 displayed the calibration curves of the nomogram in both cohorts. The nomogram yielded an accuracy of 83% (sensitivity, 81%; specificity, 85%) in the training cohort and 84% (sensitivity, 65%; specificity, 94%) in the test cohort. Examples of using the nomogram to predict the risk of LN metastasis were presented in Fig. 5.

### Clinical usefulness of the radiomics model and nomogram

DCA displayed that both the nomogram and radiomics model would offer net benefits over the “treat-all” or “treat-none”

**Fig. 4** Calibration curves of the nomogram in the training cohort (**a**) and test cohort (**b**). The 45° dotted line represents a perfect prediction. The solid line represents the predictive performance of the nomogram. The solid line has a close fit to the dotted gray line, which indicates good predictive capability of the nomogram. The blue belt represents the 95% CI of the predictive performance of the nomogram



scheme within a certain range of threshold (radiomics model, between 20 and 90%; nomogram, between 20 and 95%) in the training cohort (Fig. 6a). Similar results could be found in the test cohort (radiomics model, 30% and 90%; nomogram, 30% and 95%) (Fig. 6b).

### Discussion

In the present study, we developed and validated a CT-based radiomics nomogram for the preoperative prediction of LN metastasis in patients with gastric cancer. The radiomics nomogram holds the potential to facilitate a noninvasive individualized preoperative identification of a higher risk of LN metastasis in gastric cancer.

Accurate prediction of LN status is significant for selection of optimal therapeutic plan in patients with gastric cancer. Imaging plays a crucial role in assessing LN stage in clinical practice [38]. Nevertheless, it is still challenging in clinical practice by routinely used imaging modalities such as endoscopy ultrasonography or CT. The documented accuracy was 64% for endoscopy ultrasonography and ranged from 61 to 64% for CT in the distinction of LN metastasis [7, 10, 39]. In the current study, routine CT displayed similar capability with the accuracy of about

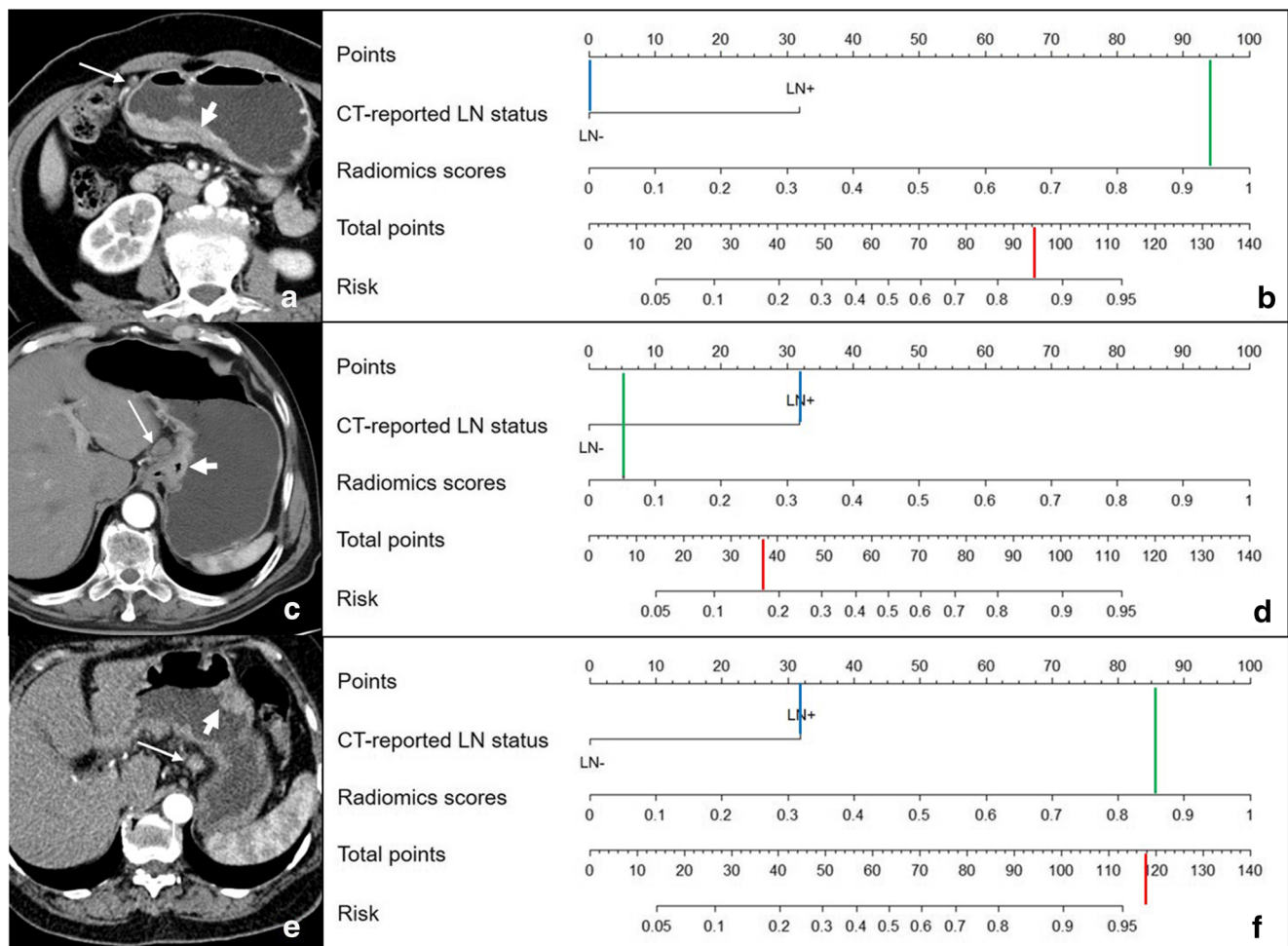


**Fig. 5** Examples of using the nomogram to predict the individual risk of LN metastasis by manually placing straight lines across the diagram. Three steps are required to obtain individual risk. First, draw vertical lines for each of the variable of the patients (CT-reported LN status: blue lines, radiomics score, green lines). Then, sum up the values intersected by the lines on the “Points” scale to obtain total points. Finally, draw a vertical line (the red lines on **b**, **d**, and **f**) the “Total points” scale to read the “Risk” of LN metastasis. **a**, **b** A 62-year-old female with gastric cancer (**a**, arrowhead). A small (diameter, 5 mm) LN (**a**, white arrow) was identified; all the other LNs were smaller than this one and not displayed on the figure. The radiomics score was 0.94. Vertical lines of each variable were drawn. The values on the “Points” scale intersected by the lines were added to obtain total points ( $0 + 94 = 94$ ). The graph revealed that the risk of LN metastasis was about 86% by drawing a vertical line on the “Total points” scale. Postoperative pathology proved the positive LN metastasis. **c**, **d** A 70-year-old male with

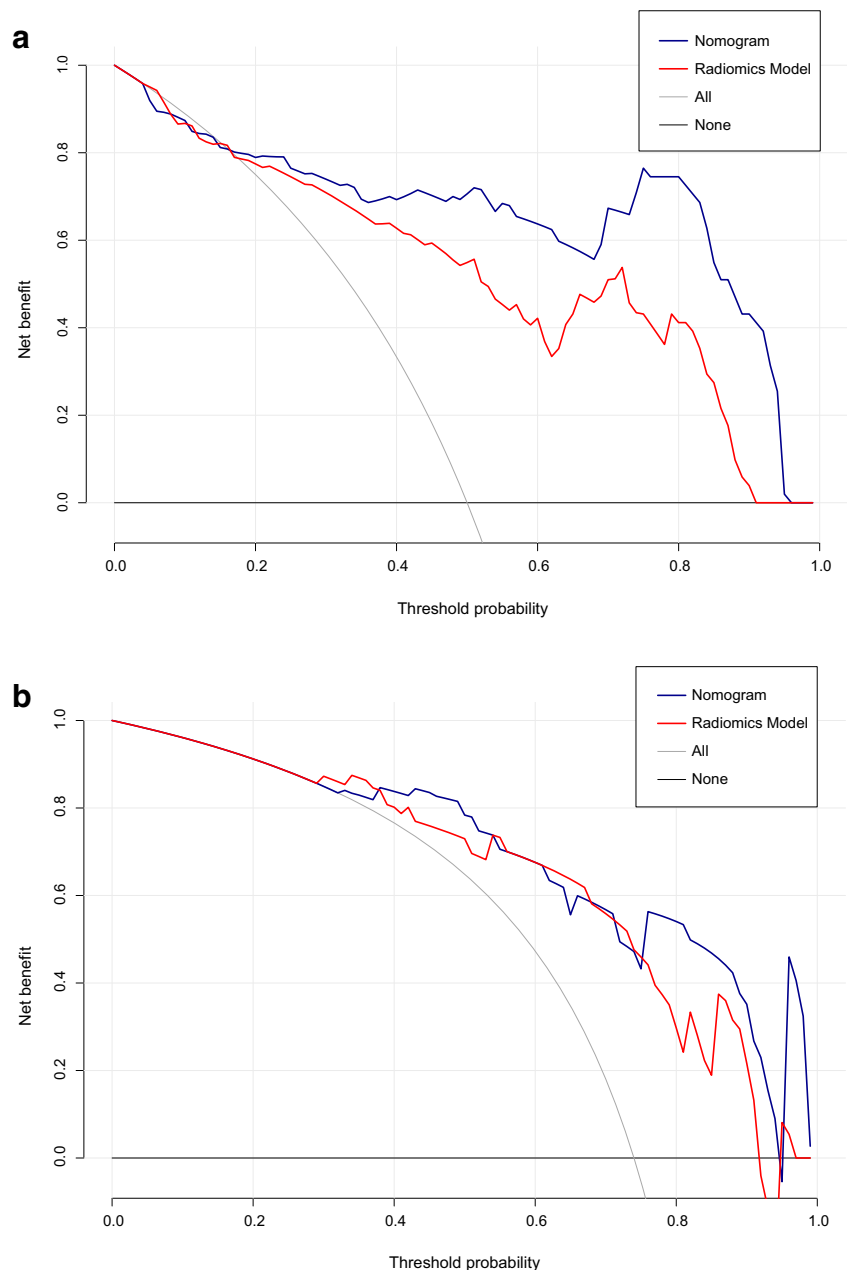
gastric cancer (**c**, arrowhead). An enlarged (diameter, 13 mm) LN (**c**, white arrow) was found. Routine CT reported positive LN metastasis. The radiomics score was 0.0615. Total points ( $32 + 5 = 37$ ) were obtained by calculating the sum of values on the “Points” scale intersected by the vertical lines of each variable. The risk of LN metastasis turned out to be about 18% by drawing a vertical line on the “Total points” scale. Postoperative pathology revealed that the patient has negative LN metastasis. **e**, **f** A 70-year-old female with gastric cancer (**e**, arrowhead). An enlarged (diameter, 12 mm) LN (**e**, white arrow) was detected. Conventional CT reported positive LN metastasis and the radiomics score was 0.876. Total points ( $32 + 86 = 118$ ) were calculated by combining the values on the “Points” scale intersected by the lines of each variable. After drawing a vertical line on the “Total points” scale, the nomogram displayed that the risk of LN metastasis was over 95%. Pathological examination validated the LN metastasis

62%. Recently, newly emerged radiomics have made it possible to predict LN status using the features of the primary tumor. The works conducted by Liu et al [20, 21] revealed that whole-lesion-based apparent diffusion coefficient histograms were valuable in the discrimination of LN metastasis with the best accuracy reaching 82.3%. While CT is more widely used and serves as the standard-of-care imaging tool for the preoperative evaluation of LN status, building radiomics models using features

extracted from routinely acquired contrast CT images could be more convenient and efficient. Our study revealed that the CT-based radiomics model showed good performance in discriminating LN metastasis with AUCs of 0.844 and 0.837 in the training and test cohorts, respectively. Besides, the model outperformed routine CT in the discrimination of cases with LN metastasis, with the accuracy increased to 80–84%. The work conducted by Feng et al [40] described that the radiomics model based on support



**Fig. 6** DCA for the nomogram and radiomics model in training cohort (a) and test cohort (b). The net benefit versus the threshold probability is plotted. Gray line represents the assumption that all patients have LN metastasis. Black line represents the assumption that all patients have negative LN metastasis. Red curve represents the radiomics model. Blue curve represents the nomogram. The *x*-axis shows the threshold probability. The *y*-axis shows the net benefit. A model is only clinically useful if it has a higher net benefit than the default treat-all (all cases have LN metastasis) and treat-none (none of the cases have LN metastasis) strategies. It is clear from the graph that the radiomics model and nomogram are superior to either treat-all or none strategy within certain ranges of risk threshold



vector machine algorithm displayed an AUC of 0.824 and 0.764 in the training and test cohorts, respectively. And the model exhibited an accuracy of 76.4% in the training cohort and 71.2% in the test cohort, which was also superior to routine CT in the distinction of LN metastasis. Although with different machine learning methods, the work by Feng et al [40] and ours rendered similar results that the radiomics approach holds the potential to enrich image interpretations and supplements the routine CT in the evaluation of LN status in gastric cancer.

Furthermore, this study also constructed an easy-to-use, graphical analog computation device—the nomogram, which allows clinicians to obtain results quickly and

reliably by simply drawing several lines. The work carried out by Li et al [41] developed a nomogram based on the iodine concentration of the tumor and Borrmann classification for the distinction of LN metastasis in patients with gastric cancer, which yielded AUCs of 0.760 and 0.793 and accuracies of 0.700 and 0.757 in the training and test cohorts, respectively. In contrast, the radiomics-based nomogram in the present study showed higher AUCs of 0.886 and 0.881 in the training and test cohort, as well as higher accuracy of 84% in both cohorts. The superior performance in this study was presumably attributable to the inclusion of the radiomics scores, which incorporated numerous quantitative features, especially parameters not

easily visible by simple visual analysis or measured by routine imaging tools. The nomogram carries great clinical significance in assisting clinicians for the selection of appropriate candidates for NAC treatment. Despite the promise in downgrading of the disease and improving the radical resection rate, evidence-based demonstration of a survival benefit of NAC compared with surgery alone is absent until now. A problem with intensive NAC is the possible inclusion of patients who may be curable by surgery alone experiencing grave adverse events from unnecessary chemotherapy [2]. Identification of the presence of LN metastasis serves as a key point in the selection of appropriate candidates for NAC therapy [2, 5]. Both the radiomics model and nomogram in the current study yield excellent performance for the distinction of LN metastasis and could offer net benefits over the “treat-all” or “treat-none” strategy within certain threshold probability.

The study had several limitations. Firstly, due to the retrospective design of the study, carcinoembryonic antigen results close to the CT scanning were performed outside our institution and not available for a subset of patients; thus, they were not included. Secondly, the study focused only on the binary classification of patients with negative or positive LN metastasis. The role of radiomics in the prediction of the detailed stage (N1–N3b) and anatomical location (16 stations) of LN metastasis was not investigated which merits further studies. Thirdly, the study only included a small number of subjects; future researches with larger population and external validation would be warranted. Finally, the radiomics features were extracted based on three-dimensional VOIs, which were labor-intensive, and further studies using two-dimensional region-of-interest-based features should be explored.

The study proved that radiomics nomogram might hold promise in the preoperative individualized prediction of LN metastasis in patients with gastric cancer.

**Acknowledgments** We would like to appreciate our co-author Yang Yu from the Siemens Healthineers for assisting in radiomics model construction and statistical analysis. The authors also acknowledge Wei Han from the Department of Epidemiology and Biostatistics, Institute of Basic Medical Sciences, Chinese Academy of Medical Sciences/School of Basic Medicine, Peking Union Medical College, for his kind help for statistical analysis.

**Funding** The study was funded by National Public Welfare Basic Scientific Research Program of the Chinese Academy of Medical Sciences (Grant Nos. 2018PT32003 and 2017PT32004).

## Compliance with ethical standards

**Guarantor** The scientific guarantor of this publication is Prof. Zheng-yu Jin.

**Conflict of interest** One of the co-authors, Yang Yu, is an employee of Siemens Healthineers. The other authors of this manuscript declare no

relationships with any companies, whose products or services may be related to the subject matter of the article.

**Statistics and biometry** Our co-author Yang Yu and Wei Han from the Department of Epidemiology and Biostatistics, Institute of Basic Medical Sciences, Chinese Academy of Medical Sciences/School of Basic Medicine, Peking Union Medical College, kindly provided statistical advice for this manuscript.

**Informed consent** Written informed consent was waived by the Institutional Review Board.

**Ethical approval** Institutional Review Board approval was obtained.

## Methodology

- retrospective
- diagnostic or prognostic study
- performed at one institution

## References

1. Bray F, Ferlay J, Soerjomataram I, Siegel RL, Torre LA, Jemal A (2018) Global cancer statistics 2018: GLOBOCAN estimates of incidence and mortality worldwide for 36 cancers in 185 countries. *CA Cancer J Clin* 0:1–31
2. Fukagawa T, Katai H, Mizusawa J et al (2018) A prospective multi-institutional validity study to evaluate the accuracy of clinical diagnosis of pathological stage III gastric cancer (JCOG1302A). *Gastric Cancer* 21:68–73
3. Smyth EC, Verheij M, Allum W, Cunningham D, Cervantes A, Arnold D (2016) Gastric cancer: ESMO clinical practice guidelines for diagnosis, treatment and follow-up. *Ann Oncol* 27:v38–v49
4. National Comprehensive Cancer Network (2018) National Comprehensive Cancer Network (NCCN) clinical practice guidelines in oncology: gastric cancer (Ver. 2). NCCN. Bethesda. Available via: <http://www.nccn.org/> Accessed at 11 Oct 2018
5. Japanese Gastric Cancer Association (2018) Japanese gastric cancer treatment guidelines (ver. 5). Japanese Gastric Cancer Association. Tokyo. Available via <https://www.kanehara-shuppan.co.jp/> Accessed at 11 Oct 2018
6. Kodera Y (2017) Neoadjuvant chemotherapy for gastric adenocarcinoma in Japan. *Surg Today* 47:899–907
7. Kim AY, Kim HJ, Ha HK (2005) Gastric cancer by multidetector row CT: preoperative staging. *Abdom Imaging* 30:465–472
8. Kinner S, Maderwald S, Albert J et al (2013) Discrimination of benign and malignant lymph nodes at 7.0T compared to 1.5T magnetic resonance imaging using ultrasmall particles of iron oxide: a feasibility preclinical study. *Acad Radiol* 20:1604–1609
9. Park HS, Kim YJ, Ko SY et al (2012) Benign regional lymph nodes in gastric cancer on multidetector row CT. *Acta Radiol* 53:501–507
10. Kim HJ, Kim AY, Oh ST et al (2005) Gastric Cancer staging at multi-detector row CT gastrography: comparison of transverse and volumetric CT scanning. *Radiology* 236:879–885
11. Jin EH, Lee DH, Jung SA et al (2015) Clinicopathologic factors and molecular markers related to lymph node metastasis in early gastric cancer. *World J Gastroenterol* 21:571–577
12. Xu YY, Huang BJ, Sun Z, Lu C, Liu YP (2007) Risk factors for lymph node metastasis and evaluation of reasonable surgery for early gastric cancer. *World J Gastroenterol* 13:5133–5138
13. Merkow RP, Bilimoria KY, Keswani RN et al (2014) Treatment trends, risk of lymph node metastasis, and outcomes for localized esophageal cancer. *J Natl Cancer Inst* 106. <https://doi.org/10.1093/jnci/dju133>

14. Lambin P, Rios-Velazquez E, Leijenaar R et al (2012) Radiomics: extracting more information from medical images using advanced feature analysis. *Eur J Cancer* 48:441–446
15. Kumar V, Gu Y, Basu S et al (2012) Radiomics: the process and the challenges. *Magn Reson Imaging* 30:1234–1248
16. Lambin P, Leijenaar RTH, Deist TM et al (2017) Radiomics: the bridge between medical imaging and personalized medicine. *Nat Rev Clin Oncol* 14:749–762
17. Ba-Ssalamah A, Muin D, Scherthaner R et al (2013) Texture-based classification of different gastric tumors at contrast-enhanced CT. *Eur J Radiol* 82:e537–e543
18. Ma Z, Fang M, Huang Y et al (2017) CT-based radiomics signature for differentiating Borrmann type IV gastric cancer from primary gastric lymphoma. *Eur J Radiol* 91:142–147
19. Liu S, Liu S, Ji C et al (2017) Application of CT texture analysis in predicting histopathological characteristics of gastric cancers. *Eur Radiol* 27:4951–4959
20. Liu S, Zhang Y, Chen L et al (2017) Whole-lesion apparent diffusion coefficient histogram analysis: significance in T and N staging of gastric cancers. *BMC Cancer* 17:665. <https://doi.org/10.1186/s12885-017-3622-9>
21. Liu S, Zhang Y, Xia J et al (2017) Predicting the nodal status in gastric cancers: the role of apparent diffusion coefficient histogram characteristic analysis. *Magn Reson Imaging* 42:144–151
22. Zhang Y, Chen J, Liu S et al (2017) Assessment of histological differentiation in gastric cancers using whole-volume histogram analysis of apparent diffusion coefficient maps. *J Magn Reson Imaging* 45:440–449
23. Giganti F, Antunes S, Salerno A et al (2017) Gastric cancer: texture analysis from multidetector computed tomography as a potential preoperative prognostic biomarker. *Eur Radiol* 27:1831–1839
24. Giganti F, Marra P, Ambrosi A et al (2017) Pre-treatment MDCT-based texture analysis for therapy response prediction in gastric cancer: comparison with tumour regression grade at final histology. *Eur J Radiol* 90:129–137
25. Hou Z, Yang Y, Li S et al (2018) Radiomic analysis using contrast-enhanced CT: predict treatment response to pulsed low dose rate radiotherapy in gastric carcinoma with abdominal cavity metastasis. *Quant Imaging Med Surg* 8:410–420
26. Li W, Zhang L, Tian C et al (2018) Prognostic value of computed tomography radiomics features in patients with gastric cancer following curative resection. *Eur Radiol*. <https://doi.org/10.1007/s00330-018-5861-9>
27. Japanese Gastric Cancer Association (2011) Japanese classification of gastric carcinoma: 3rd English edition. *Gastric Cancer* 14:97–100
28. Beam CA (1992) Strategies for improving power in diagnostic radiology research. *AJR Am J Roentgenol* 159:631–637
29. Gillies RJ, Kinahan PE, Hricak H (2016) Radiomics: images are more than pictures, they are data. *Radiology* 278:563–577
30. Suthaharan S (2016) Machine learning models and algorithms for big data classification: thinking with examples for effective learning, 1st edn. Springer US, New York
31. Zhang N, Yang G, Gao Z et al (2019) Deep learning for diagnosis of chronic myocardial infarction on nonenhanced cardiac cine MRI. *Radiology*. <https://doi.org/10.1148/radiol.2019182304>
32. Nicosia G, Pardalos P, Giuffrida G, Umeton R (2018) Machine learning, optimization, and big data: third international conference, MOD 2017, Volterra, Italy, September 14–17, 2017, revised selected papers Springer International Publishing, Switzerland
33. Aerts HJ, Velazquez ER, Leijenaar RT et al (2014) Decoding tumour phenotype by noninvasive imaging using a quantitative radiomics approach. *Nat Commun* 5:4006. <https://doi.org/10.1038/ncomms5006>
34. Yuan M, Zhang YD, Pu XH et al (2017) Comparison of a radiomic biomarker with volumetric analysis for decoding tumour phenotypes of lung adenocarcinoma with different disease-specific survival. *Eur Radiol* 27:4857–4865
35. Sandri M, Zuccolotto P (2006) Data analysis, classification and the forward search, 1st edn. Springer, Berlin Heidelberg
36. Hintze J, Nelson R (1998) Violin plots: a box plot-density trace synergism. *Am Stat* 52:181–184
37. Van Calster B, Wynants L, Verbeek JFM et al (2018) Reporting and interpreting decision curve analysis: a guide for investigators. *Eur Urol* 74:796–804
38. Giganti F, Tang L, Baba H (2018) Gastric cancer and imaging biomarkers: part 1 - a critical review of DW-MRI and CE-MDCT findings. *Eur Radiol* 29:1743–1753
39. Cardoso R, Coburn N, Seevaratnam R et al (2012) A systematic review and meta-analysis of the utility of EUS for preoperative staging for gastric cancer. *Gastric Cancer* 15(Suppl 1):S19–S26
40. Feng QX, Liu C, Qi L et al (2019) An intelligent clinical decision support system for preoperative prediction of lymph node metastasis in gastric cancer. *J Am Coll Radiol*. <https://doi.org/10.1016/j.jacr.2018.12.017>
41. Li J, Fang M, Wang R et al (2018) Diagnostic accuracy of dual-energy CT-based nomograms to predict lymph node metastasis in gastric cancer. *Eur Radiol* 28:5241–5249

**Publisher's note** Springer Nature remains neutral with regard to jurisdictional claims in published maps and institutional affiliations.